Accepted Manuscript
https://doi.org/10.1016/j.icheatmasstransfer.2019.104456

Heat transfer enhancement through periodic flow area variations in microchannels

Kai Xian Cheng [1, *], Zi Hao Foo[*], Kim Tiow Ooi

School of Mechanical and Aerospace Engineering, Nanyang Technological University, 50 Nanyang Avenue, Singapore 639798, Singapore

* Joint lead authors

[1] kcheng003@e.ntu.edu.sg (Corresponding author)

Abstract: In this study, annular microchannels with a microscale gap of 300 µm were implemented through the concentric superposition of two macro-sized cylinders. Flow area variations along the streamwise direction were created by introducing sinusoidal wave profiles on either the inner or outer wall of the annular gap while keeping the other wall flat. These variations introduced re-entrant effects along the flow direction. Numerical studies using the finite volume method were performed to elucidate the single-phase, steady-state thermal and hydrodynamic performances of the wavy channels, using water as the fluid medium, with an operating Reynolds number range of 800 – 2200. The predicted results were validated using the available measured data and classical correlations. This study demonstrated the viability of attaining enhanced heat transfer rates of up to 360% of the original straight channel through the inducement of flow area variations with single wavy-walled channels. Despite magnifications of the friction factors, the single wavy-walled channels attained a 120% increment in heat transfer coefficient when evaluated at the same pumping power. Overall, single-walled wavy passages were deemed suitable for heat exchanger designs demanding very high heat removal rates and efficiencies while the conventional serpentine channels were apt for moderately enhancing heat transfer while requiring low pumping power.

Keywords: single-walled, wavy channel, heat transfer, microscale, annular

1. Introduction

Microchannel cooling technology includes the implementation of single-phase liquid cooling in micro-geometry heat dissipation elements as well as two-phase flow boiling [1]. The conventional definition of microchannels with hydraulic diameters ranging from 1 µm to 1 mm is commonly adopted [2]. While two-phase cooling techniques are superior in heat removal, the inherent flow boiling instabilities and the corresponding high pumping power consumption posed a massive hurdle for industrial implementations [3, 4]. Thus, single-phase liquid cooling remains an active field of research owing to its prospect of achieving relatively high heat transfer performance while avoiding the complexities of multi-phase flow. Subsequent reviews by Kandlikar [5], Goodling [6] and Palm [7] regarding single-phase convective heat transfer in microchannel heat sinks also stressed the industrial demand for further augmentation of the passive enhancement techniques through microscale surface features and nanofluids employment.

Since then, numerous design philosophies for heat transfer augmentation have been proposed. Among which, interest in wavy microscale passages burgeoned after Sui et al. [8] numerically attained enhanced heat transfer with minor pressure loss magnification using the same channel cross-section. Subsequent investigations on wavy channels [9, 10] elucidated that secondary flows generated due to centrifugal forces promoted fluid rotation, improving flow mixing for enthalpy redistribution and an overall heat transfer enhancement. Optimisation of the wave geometry by Xie et al. [11] and Rostami et al. [12] concluded that high amplitude-to-wavelength ratios intensified the vortices, yielding better cooling performances. Width-tapered channels were reported to reduce the overall thermal resistance by up to 16.7% relative to rectangular channels by Hung and Yan [13]. Concurrently, Ho et al. [14] reported that diverging channels exhibited greater Nusselt numbers while lowering the overall pressure losses. Sakanova et al. [15] reported that higher amplitude and shorter wavelength wavy-walled channels developed lower overall thermal resistance while Ghaedamini et al. [3] investigated the geometric effects of phase shifts and channel constrictions in converging-diverging wavy channels and attained enhanced thermal performance of 20%. Double-layering of microchannel heat sinks were also optimised for minimal thermal resistances through a three-dimensional conjugate gradient method by Leng et al. [16]. Harikrishnan and Tiwari [17] concluded that the implementation of skewed wavy channels intensified the strength of the vortices. Also, twisting of the sinusoidal wavy channels was reported by Hasis et al. [18] to enhance heat removal by up to 30%. Heat transfer enhancement through the alteration of the amplitude and wavelength along the flow direction was investigated by Lin et al. [19] as well. Lastly, nanofluids employment in wavy channels, corrugated channels and circular tubes were proven to be viable in augmenting heat transfer by Dominic et al. [20], Khoshvaght-Aliabadi and Sahamiyan [21], and Ho et al. [22] respectively.

While there are numerous studies concerning the thermo-hydraulic performance enhancement enabled by serpentine wavy channels, this study examines the possibility of realising re-entrant effects through flow area variations. This configuration is created by introducing a wave profile on one of the walls in an annular channel. This is in light that asymmetrical wavy plates were reported to be capable of inducing streamline vortices [23], a potential mechanism for further enhancement of heat transfer performances in microscale channels. On top of that, there is recent interest in the implementation of microchannel heat sinks using relatively low-cost conventional manufacturing [24-28]. The microscale heat transfer effects were realised by the concentric superposition of two macro-sized cylinders [29], as depicted in Figure 1. Given the axial symmetry of wave profiles, conventional machining methods, such as turning, can be readily implemented into this configuration.

Thus, the present study investigates the feasibility of employing single wavy-walled passages to attain enhanced microscale heat transfer while utilising conventional manufacturing techniques, given its potential applications due to its ease of deployment and production [30, 31]. Also, while existing studies on serpentine wavy channels have demonstrated potential in achieving high thermo-hydraulic performances, there are no direct comparisons between single wavy-walled and serpentine channels available in the literature presently.

Hence, this paper studies the effects of both single wavy-walled and serpentine channels, with a mean channel gap of 300 μm, on the heat transfer and flow characteristics of the microscale flow in an annular channel. A three-dimensional model employing water at a Reynolds number range from 800 - 2200, with an average heat flux of 50 W cm^{-2}, is used to analyse the respective thermal and hydrodynamic performances, using the finite volume method. Numerical validation is performed using existing experimental results and classical correlations. The novelty of this study lies in the elucidation of the relative thermal and hydrodynamic performances and the corresponding heat transfer enhancement mechanisms of the respective implementations, under the same heat flux conditions, serving to guide engineering designs of industrial heat exchangers.

2. Numerical Model

2.1 Geometry Definition and Modelling

In this study, the straight annular microchannel was formed through the concentric superposition of a 19.4 mm insert, with no wave protrusions, within a 20.0 mm hollow cylinder, as depicted in Figure 1. Fluid flow was restricted to the 300 μm microscale gap and the length of the annular channel was 30 mm, where heat was supplied to the fluid from the external cylinder.

To induce periodic flow area variations using single wavy-walled channels, sinusoidal waves were introduced on the inner, non-heating surface of the insert or the internal, heating surface of the exterior hollow cylinder, thereby constituting the ‘Wavy-Insert’ and ‘Wavy-Heater’ configurations respectively, as illustrated in Figures 2(b) and (c). The amplitudes and wavelengths of the sinusoidal waves were 0.15 mm and 3 mm respectively, as given in Table 1, corresponding to a minimum channel gap of 150 μm and 10 complete waveforms along the 30 mm long channel. The conventional wavy channel, coined here as the ‘Wavy-Serpentine’ configuration, was implemented by introducing in-phase sinusoidal waves on both surfaces of the annular channel, as illustrated in Figure 2(d). Given that the heat transfer areas of the ‘Wavy-Heater’ and ‘Wavy-Serpentine’ configurations were 2.4% greater due to the wave profile on the heating domain, an effective heat flux of 50 W cm^{-2} was applied normally to the external cylinder’s surface as the boundary condition for all configurations to ensure

valid comparisons [32]. The mean microscale gap for all configurations was kept constant at 300 μm, as shown in Table 1, to maintain a constant volume of fluid passing through the channel, ensuring that the average hydraulic diameters and subsequently, the average Reynolds number of each configuration were equal for a given flow rate, allowing for juxtaposition of the overall thermal performances [25].

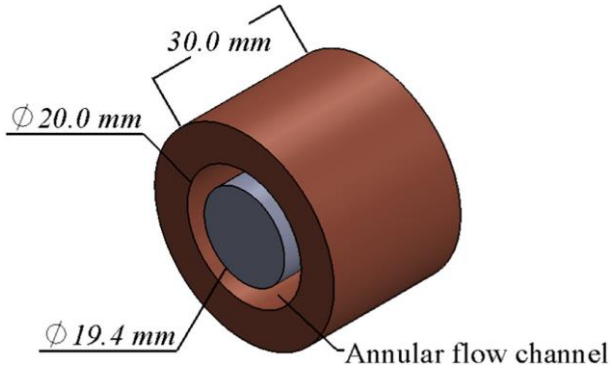

Figure 1 Straight annular channel with a gap size of 300 μm. Adapted with permission from [24].

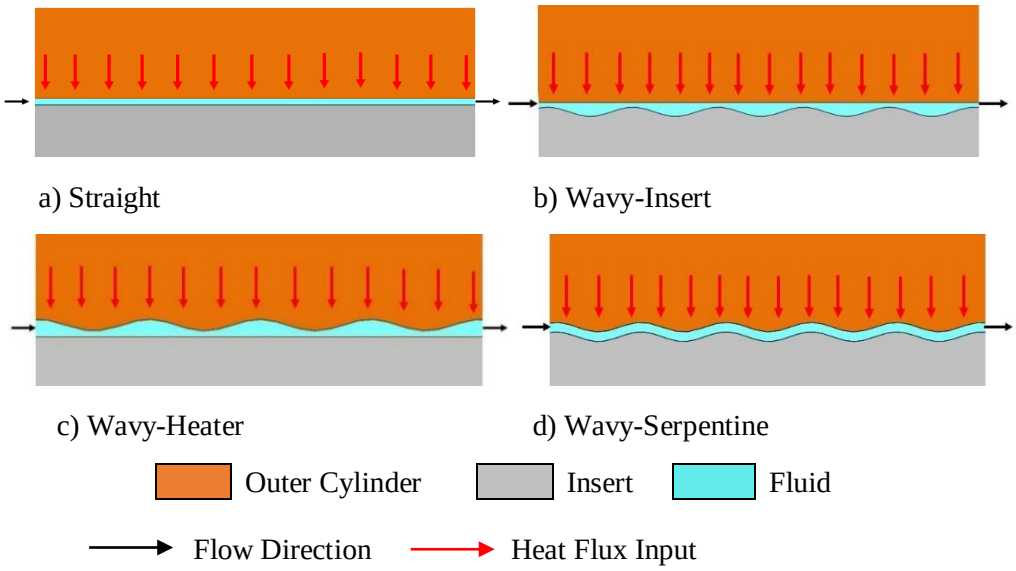

Figure 2 Illustrations of the single-walled and serpentine wavy channels.

Table 1 Nomenclature and wave parameters of the channel configurations.

Configuration	Amplitude/mm	Wavelength/ mm	Minimum channel gap/μm	Maximum channel gap/μm
Straight	-	-	300	300
Wavy-Insert	0.15	3.0	150	450
Wavy-Heater	0.15	3.0	150	450
Wavy-Serpentine	0.15	3.0	300	300

Numerical simulations were performed using a three-dimensional model to investigate the steady-state flow and heat transfer characteristics in the various wavy annular channels, for the range of Re from 800 to 2200. The conjugate model was designed based on the physical experimental test module adopted by Foo et al. [27], as shown in Figure 3, to allow for the validation of the numerical results. The various wavy configurations depicted in Figure 2 were implemented within the microscale gap, as depicted by the red box in Figure 3. The following boundary conditions and simplifications were applied to simulate experimental conditions and reduce computational requirements:

Numerical Simplifications

a. Single-phase, steady-state, incompressible liquid flow
b. Negligible body forces and gravitational effects
c. Negligible internal heat generation and radiative heat transfer
d. Constant thermodynamic properties for the solid and fluid domains
e. $1/8^{th}$ model owing to the axial symmetry of the annular channel

Boundary Conditions

a. A system inlet temperature boundary of 28°C and system outlet pressure of 101 kPa (absolute)
b. Free convection at the outer, exposed surfaces of the test system with a heat transfer coefficient of 8 W m^{-2} K^{-1} [33] at an ambient temperature of 30 °C
c. Average heat flux application of 50 W cm^{-2} on the copper-fluid boundary and conservative heat flux between all solid-solid and solid-fluid interfaces
d. No-slip conditions on all solid-fluid interfaces

The thermodynamic properties of the solid domains were evaluated at the ambient temperature of 30°C from the REFPROP software, as given in Table 2, while the properties of the fluid were determined at the mean bulk fluid temperature, based on energy balance, using Helmholtz-free energy formulations [34] adapted from the International Association for the Properties of Water and Steam (IAPWS) [35].

The geometry was discretised using tetrahedron elements of quadratic order and high orthogonal quality was ensured [36], as illustrated in Figures 4(a) to (d). To further refine the mesh quality and resolution near the fluid-solid boundary and model the boundary layers with high precision, inflation layers have been extruded normally with more than 10 nodes, as suggested by literature [36]. The enabling of the General Grid Interface function also connected the non-matching nodes between the solid and fluid domain meshes.

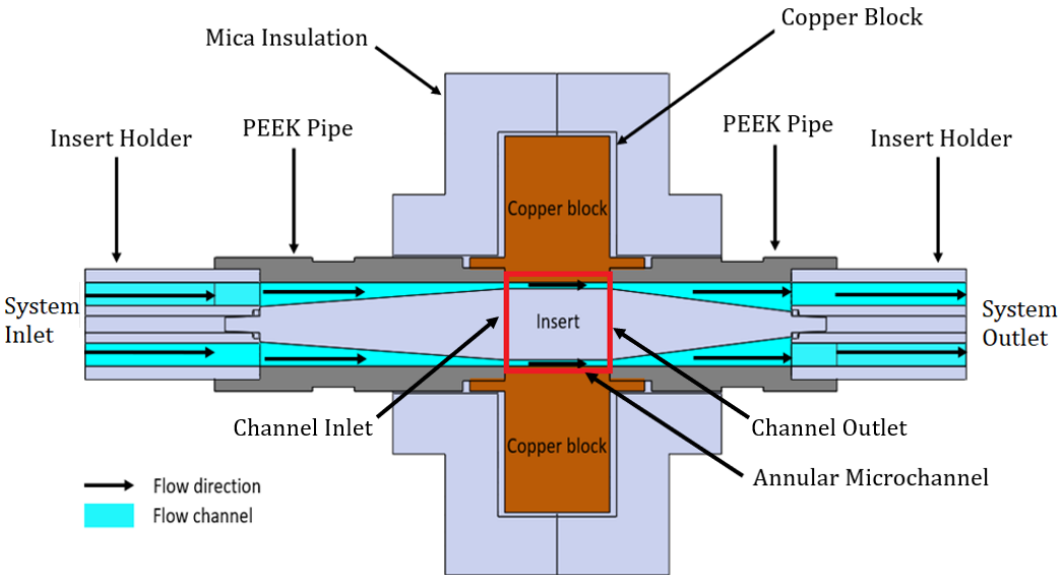

Figure 3 Schematics and components of the test module.

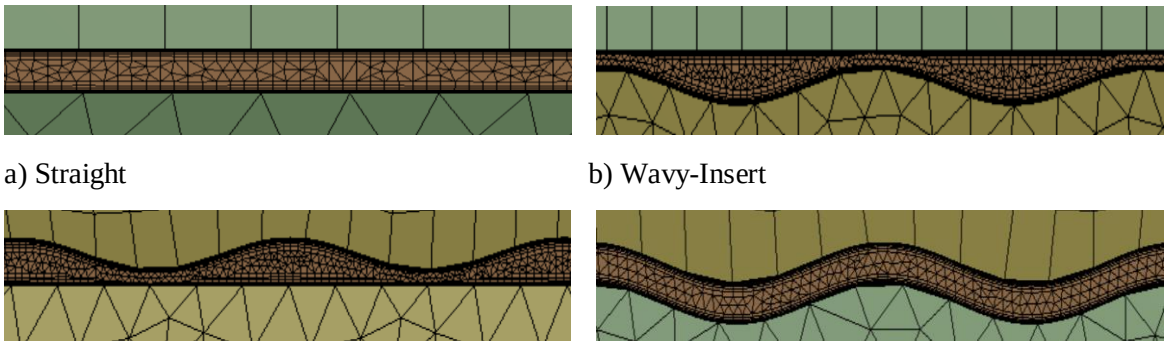

a) Straight b) Wavy-Insert

c) Wavy-Heater d) Wavy-Serpentine

Figure 4 Mesh of the wavy configurations within the annular microchannel.

2.2 Mathematical modelling and data reduction

The governing equations [36] which included the continuity equation, Reynolds-averaged Navier-Stokes equations and, energy equations in both solid and fluid domains were solved using CFX, employing a pressure-velocity coupled, vertex-centred finite volume method, complemented with spatial discretization using the high-resolution method.

To accurately model the streamline vortices caused by flow perturbations due to the wave geometries, as depicted in literature [8-10], the k-ω Shear Stress Transport (SST) model has been adopted to resolve the turbulence closure problem [36], owing to its ability to accurately predict the pressure-induced separation and the viscous-inviscid interaction within the flow [36] and resolve the thermal and velocity boundary layers accurately [37]. The convergence of the solutions was only considered once the root-mean-square residuals reduced to the order of 10^{-6} for all variables.

Table 2 Thermophysical properties of the solid domain of the numerical system.

Material	ρ (kg m^{-3})	c_p (J kg^{-1} K^{-1})	k (W m^{-1} K^{-1})
Copper	8.933 x 10^6	385	401
Mica	2100	500	0.31
PEEK	1400	1800	0.92
Stainless Steel	7.854 x 10^6	434	60.5

The inlet bulk fluid temperature was set at 28 °C as the boundary condition. The outlet bulk fluid temperatures at the channel outlet, from Figure 3, were evaluated at the mass flow average:

$$T_{out} = \frac{1}{\rho V A_{cr}} \int_{A_{cr}} T \rho u dA \tag{1}$$

$$V = \frac{1}{\rho A_{cr}} \int_{A_{cr}} u \rho dA \tag{2}$$

The mean fluid temperature was the average of the channel inlet and outlet temperatures:

$$T_{f,m} = \frac{T_{in} + T_{out}}{2} \tag{3}$$

The sensible heat flux applied to the fluid was computed using an energy balance formulation:

$$q = \frac{\rho \dot{V} c_{p,m} \left(T_{out} - T_{in} \right)}{A_w} \tag{4}$$

The average wall temperature was computed, and the subsequent heat transfer coefficient was evaluated using Newton's law of cooling:

$$T_{w,m} = \frac{1}{A_w} \int_{A_w} T_w dA \tag{5}$$

$$\bar{h} = \frac{q}{\left(T_{w,m} - T_{f,m} \right)} \tag{6}$$

The local heat transfer coefficient was also determined using the local bulk temperatures of the fluid and wall.

$$h_x = \frac{q_x}{\left(T_{w,x} - T_{f,x} \right)} \tag{7}$$

The average Nusselt number is computed from the derived average heat transfer coefficient and hydraulic diameter:

$$D_h = D_{ch,ext} - D_{ch,int} \tag{8}$$

$$\overline{\mathrm{Nu}}_{ch} = \frac{\bar{h} D_h}{k_f} \tag{9}$$

The pressure loss across the channel inlet and outlet, depicted in Figure 3, was calculated with Equation 10. Furthermore, the pressure loss across the system inlet and outlet was also computed for experimental validation [27].

$$\Delta p_{ch} = p_{ch,in} - p_{ch,out} \tag{10}$$

$$\Delta p_{sys} = p_{sys,in} - p_{sys,out} \tag{11}$$

Following which, the Reynolds number and the Darcy friction factor were determined:

$$\mathrm{Re} = \frac{\dot{m} D_h}{A_c \mu} \tag{12}$$

$$f_{sys} = \frac{2 D_h^3 \rho (\Delta p_{sys})}{L \mu^2 \mathrm{Re}^2} \tag{13}$$

Lastly, the pumping power consumed by the microscale flow was calculated from the pressure loss and the volumetric flow rate.

$$\Omega = \dot{V} \cdot \Delta p_{ch} \tag{14}$$

2.3 Mesh Independence Test

Mesh independence tests were conducted for each configuration at the highest tested Reynolds number. The test results for the straight configuration are illustrated in Figure 5. Based on Figure 5, the mesh system with an element count of 2.6 million was chosen as the further increment of the element count by 42% (to 3.7 million) only yielded a marginal improvement in accuracy by 0.9%. Similar mesh independence results were obtained for the other 3 configurations as well.

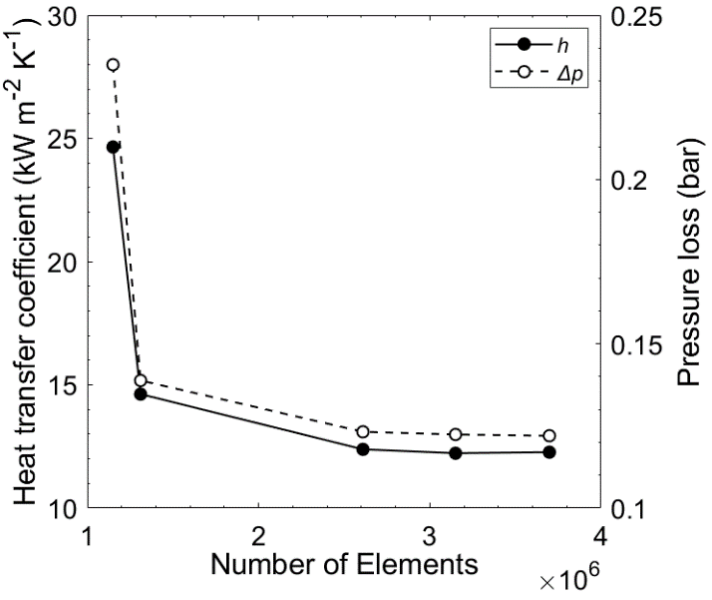

Figure 5 Mesh independence test for the straight configuration.

3. Results and Discussions

3.1 Validation of Numerical Results

Considering the theoretical dimensionless hydrodynamic and thermal entrance lengths, the flow for the straight configuration falls within the combined entrance region in this study [38]. Thus, developing laminar flow correlations for Nusselt number and friction factor of parallel plate flows, by Shah and London [38] and Muzychka [39] respectively, were juxtaposed with the predicted numerical values for the straight configuration, as depicted in Figure 6(a). Comparisons showed acceptable agreement with the approximated classical theories, registering an average and maximum underprediction of 10.5% and 10.6% for the Nusselt number and an average and maximum difference of 9.3% and 12.4% for the friction factor.

Experimental measurements from Foo et al. [27] for the straight and 'Wavy-Insert' configurations were also used to validate the numerical results, as illustrated in Figures 6(a) and (b). The maximum difference for the Nusselt numbers of the straight and 'Wavy-Insert' configurations were 12 % and 15 % respectively. Overall, the average deviations for the straight and 'Wavy-Insert' configurations are 9.7 % and 6.3 % respectively, which is within the reported uncertainty of 13.4 % [27], demonstrating good agreement with the experimental measurements. For the friction factor, the straight and 'Wavy-Insert' configuration registered a maximum difference of 15 % and 8 % respectively. The overall average difference for the two configurations were 8.3 % and 5.6 %, well within the reported uncertainty of 11.1 % [27]. Therefore, the experimental validation increased our confidence in employing the numerical model to predict and contrast the performances of the respective wavy configurations.

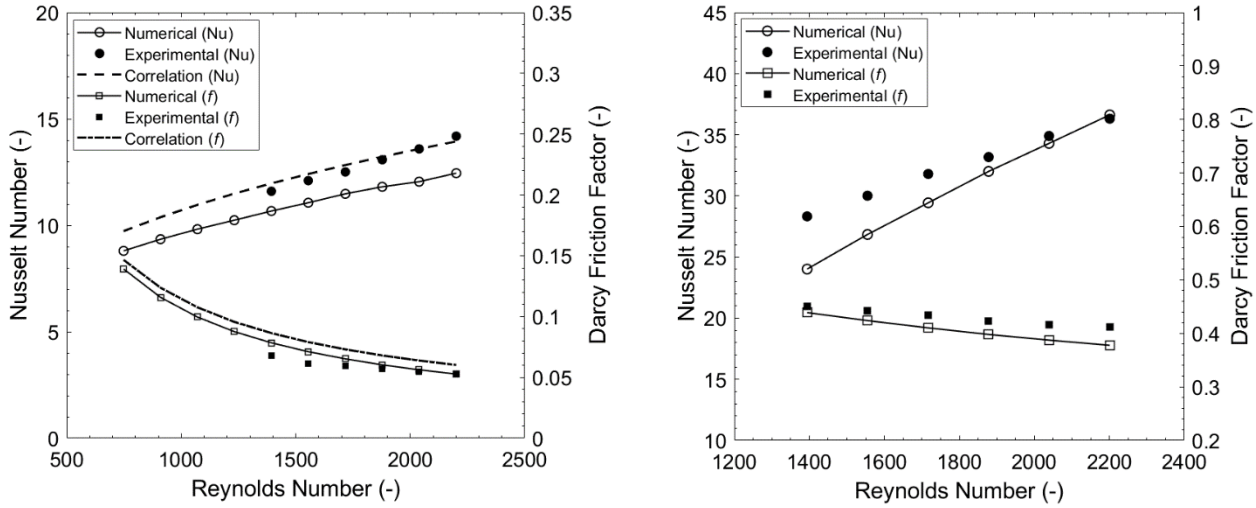

a) Straight configuration b) Wavy-insert configuration

Figure 6 Comparison between the predicted and correlated parameters.

3.2 Heat transfer Enhancements with Wavy Microscale Profiles

The average Nusselt numbers of the straight, serpentine and single wavy-walled configurations are plotted in Figure 7. Both the single wavy-walled and serpentine passages attained enhanced heat transfer performances over the straight channel. At Re of 2200, the enhancement registered by the 'Wavy-Heater' profile can be as high as 260% while the serpentine configuration registered an augmentation of 70%, relative to the straight configuration. Noteworthily, both single wavy-walled channels outperformed the serpentine channel in heat transfer for the current range of Reynolds number while the 'Wavy-Heater' consistently registered higher average Nusselt numbers over the 'Wavy-Insert' profile.

The local *h* corresponding to the operating average Reynolds number of 2200 for 5th, 6th and 7th waveforms along the channel length are presented in Figure 8 while the position coordinates are defined in Figure 9.

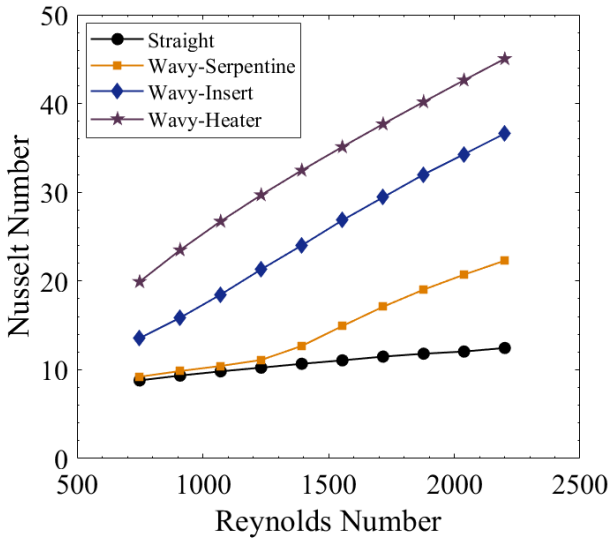

Figure 7 Nusselt number performance of the wavy annular microchannels.

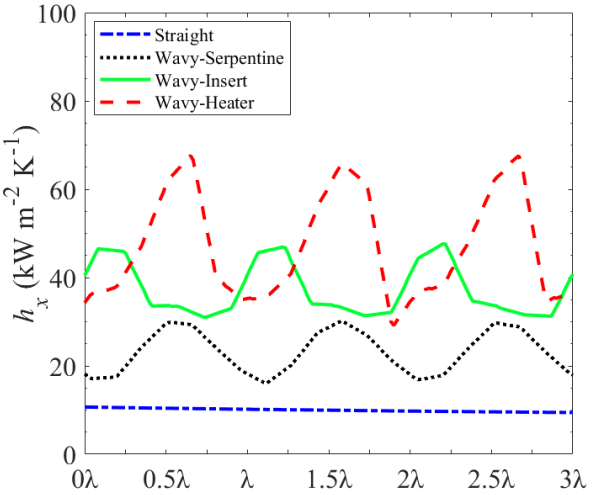

Figure 8 Local heat transfer coefficient distributions of the configurations.

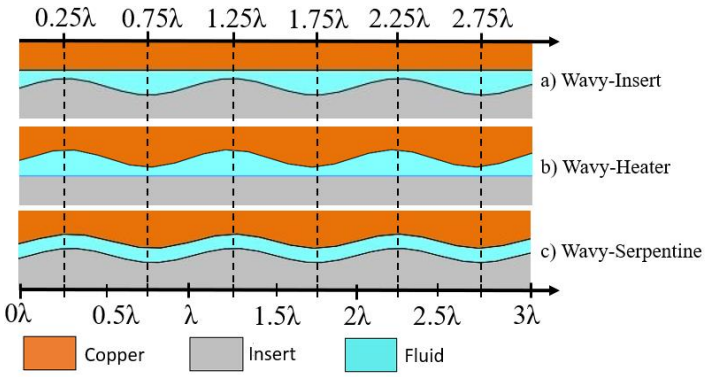

Figure 9 Position coordinates for the local heat transfer coefficients of the wavy configurations.

For the serpentine configuration, the maximum *h* is registered at 0.5λ. As the fluid flows past the bend at 0.25λ in the channel, the inertia of the flow [8, 9] led to an outward shift of the maximum velocity away from the centreline towards the heated surface after passing the peak at 0.25λ. This caused higher velocity fluid to be brought closer to the heating wall at 0.5λ, directly after the bend, leading to a thinning of the local velocity boundary layer in that region, as shown in Figure 10(b). The improved mixing due to the flow inertia contributed to the overall thinning of the thermal boundary layers [8].

For the single wavy-walled channel, 'Wavy-Insert', the constriction of the flow area at 0.25λ due to the peaks of the wave profiles induced higher fluid velocities, by virtue of mass flow conservation, as observed in Figure 10(c). The drastic increase in the local velocity gradient at the minimum flow area promoted enhanced heat removal [40] and triggered boundary layer thinning in Figure 10(c). This caused the local *h* to be consistently recorded at the peaks of the microscale wave protrusions for 'Wavy-Insert', as reflected in Figure 8. Low velocity, counter-rotating vortices were also formed following the expansion of the flow area in Figure 10(c). The fluid streamlines exiting the minimum flow area were observed to bypass the trough of the wave and carry high fluid velocities across the maximum channel gap. This resulted in high heat transfer to be observed continuously, even beyond the minimum flow area, causing relatively high *h* to be recorded even at the maximum channel gaps despite it being larger than the corresponding gap sizes found in the straight and serpentine channels. As a result, the single wavy-walled channels outperformed the serpentine channel in heat transfer across the entire channel length, amounting to the higher Nusselt numbers observed in Figure 7.

Similar channel constriction effects on the local thermal performances were present in the 'Wavy-Heater' configuration in Figure 10(d). However, as opposed to the 'Wavy-Insert' configuration, thin velocity boundary layers were already observed prior to channel constriction, at 0.5 λ. Unlike the 'Wavy-Insert' profile, the low-velocity recirculatory zones were located near the heating surface of the Wavy-Heater configuration. Therefore, the high-velocity fluid exiting the minimum flow area

bypassed the streamline vortices and came into direct contact with the copper wall at 0.5λ, inducing a region of thin velocity boundary layers on the heating wall, as depicted in Figure 10(d). The high velocity gradient at the near-wall at 0.5λ, coupled with the subsequent channel constriction at 0.75λ, led to high local *h* from 0.5λ to 0.75λ. The amalgamation of the two mechanisms in the 'Wavy-Heater' configuration led to enhanced Nusselt numbers relative to the 'Wavy-Insert' profile registered in Figures 7 and 8.

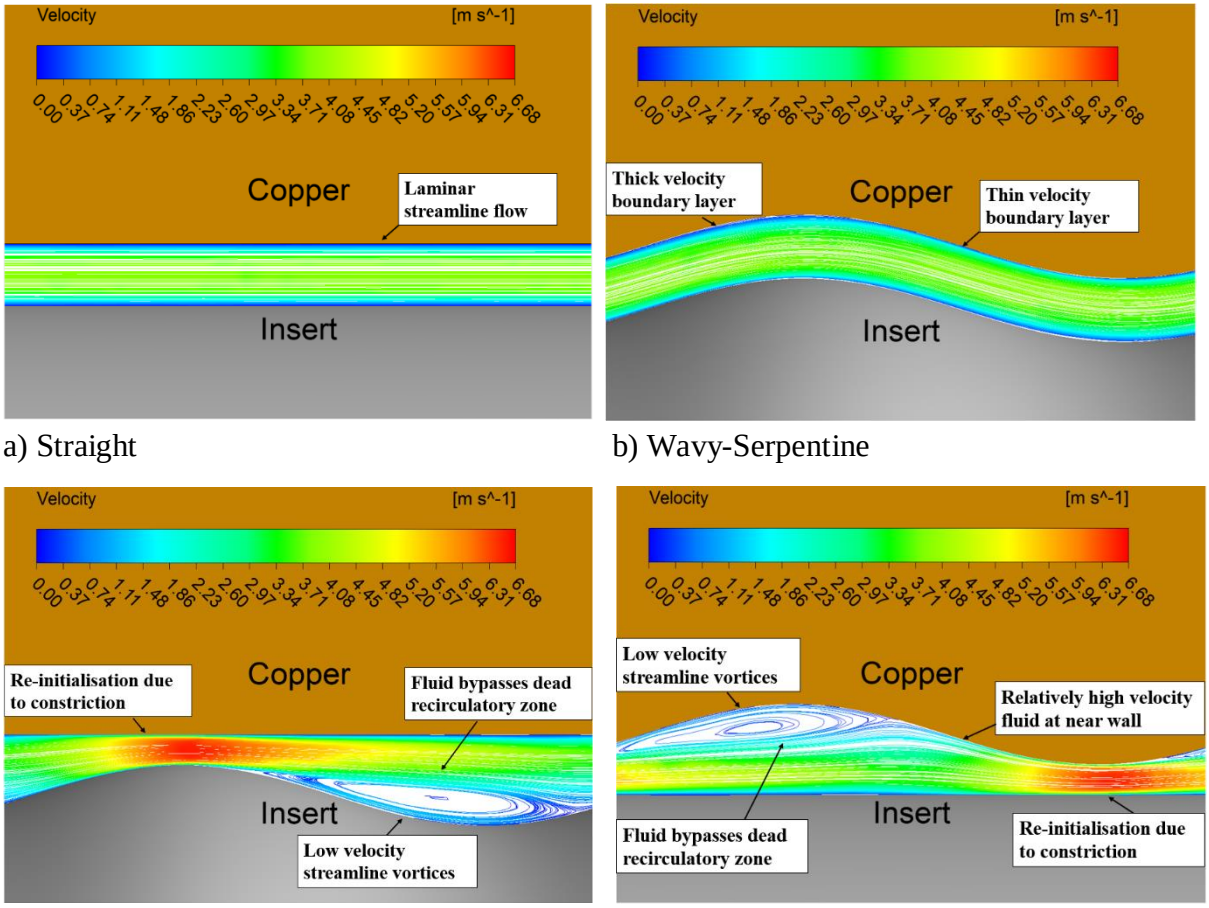

a) Straight

b) Wavy-Serpentine

c) Wavy-Insert

d) Wavy-Heater

Figure 10 Local velocity distribution and streamlines within the annular channels.

3.3 Effects on the Hydrodynamic Performance

As depicted in Figure 11, the enhancement in the heat transfer was met with an undesirable increment in the friction factor, demanding higher pumping power consumption due to the increased head loss for the wavy-profiled channels. The single wavy-walled channels recorded magnified friction factors of up to 6 times relative to the straight channel, while the serpentine channel registered a marginal 30 per cent increase in friction factors. For the single wavy-walled channels, the high velocity fluid bypassed the recirculation zones after exiting the constricted flow area in Figure 10, leading to heightened head losses to be consistently recorded at both the minimum and maximum flow cross-sections. This, in turn, led to the undesirable magnification of the friction factors. On the contrary, the

laminar streamline flow within the serpentine channel highly mimics the original straight channel and the marginal increase in friction factors can be attributed to the local head losses induced at the bends and meanders [12].

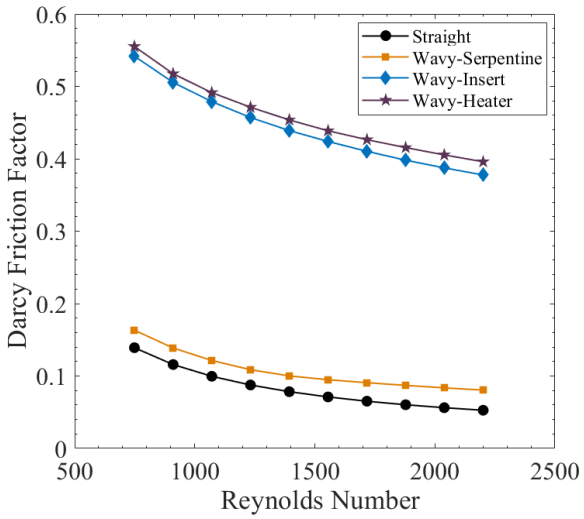

Figure 11 Friction factor performance against Reynolds number of the annular channels.

Figure 12 illustrates the increment in *h* at the same pumping power. Consistent with prior studies on serpentine channels, improvement in *h* under the same pumping power inputs of up to 10% were registered. However, under the same hydrodynamic inputs, single wavy-walled channels demonstrated superior performances relative to the conventional serpentine channels in terms of the increment in *h*, across the entire range of pumping inputs. The highest enhancement in *h* was attained by the single-walled channel, 'Wavy-Heater', across the tested range of pumping powers, with a maximum increment by 120% relative to the straight channel. The other single-walled configuration, 'Wavy-Insert', also registered moderately large enhancements in *h* by 53% when compared to the straight channel.

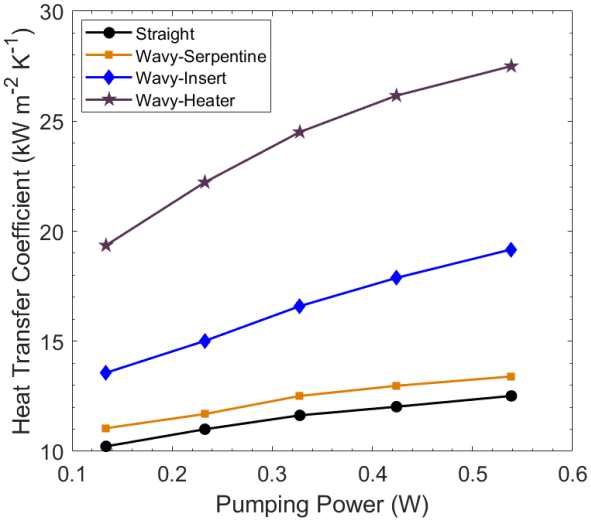

Figure 12 Heat transfer performance comparison under a constant pumping power input.

In conclusion, both single-walled and serpentine wavy passages improved the heat transfer of the flow system. Thus, the optimal configuration for industrial applications depends exclusively on the operating limitations. The conventional serpentine channels were deemed optimal for applications in industrial heat exchangers requiring low pressure losses while attaining moderate enhancement in heat transfer. On the contrary, the novel single wavy-walled configurations were suitable for employment in heat exchanger systems with high pumping power capabilities while demanding extremely high heat removal rates and thermo-hydraulic efficiencies.

4. Conclusion

In this study, a numerical approach was adopted to investigate the thermal and hydrodynamic performances of serpentine and single wavy-walled microchannels. Mesh independence tests and validation through measurement and correlations were performed to demonstrate the reliability of the numerical results. The single-phase, steady-state conjugate convective heat transfer phenomena were investigated using water as the working fluid, for the Reynolds number range of 800 – 2200. The heat transfer performances and its underlying mechanisms of the wavy annular channels were elucidated, and the increment in heat transfer coefficient was also evaluated at the same pumping power. Major findings from the study are as follows:

1. The single-walled wavy channels outperformed the serpentine channels in terms of heat transfer, registering a maximum Nusselt number of 46.2 at a Reynolds number of 2200, approximately 260% augmented relative to the original straight channel.
2. Conventional serpentine channels were capable of enhancing heat transfer up by to 79% with minor friction factor magnifications in annular channels, where the enhancement was due to the thinning of boundary layers arising from fluid inertia during channel meandering.
3. Flow area constrictions in single wavy-walled passages induced higher velocity gradients and better fluid mixing, leading to significant enhancements in heat transfer, albeit at large friction factor magnifications.
4. The introduction of single-walled waves on the heating surface of the annular channel improved the thermo-hydraulic performance to the largest extent, registering a maximum increment of heat transfer by 120% when evaluated under the same pumping power.

Nomenclature

A	Surface area (m^2)
c_p	Specific heat capacity (J kg^{-1} K^{-1})
D	Diameter (m)
D_h	Hydraulic diameter (m)
f	Darcy friction factor (-)
h	Heat transfer coefficient (kW m^{-2} K^{-1})
$\overline{h}$	Mean heat transfer coefficient (kW m^{-2} K^{-1})
k	Thermal conductivity (W m^{-1} K^{-1})
L	Length (m)
Nu	Nusselt number (-)
p	Pressure (Pa)
q	Heat flux (W m^{-2})
r^*	Radius ratio (-)
Re	Reynolds number
T	Temperature (K)
u	Local fluid velocity (m s^{-1})
V	Average Fluid Velocity (m s^{-1})

Greek symbols

ν	Kinematic viscosity (m^2 s^{-1})
ρ	Density (kg m^{-3})
τ	Stress tensor (Pa)
μ	Dynamic viscosity (Pa·s)
Ω	Pumping Power (W)

Subscripts

ch	Channel
cr	Cross-section
ext	External cylinder
f	Fluid
in	Inlet
int	Internal cylinder
m	Mean
out	Outlet
s	Straight
sys	System
w	Wall
x	Local parameter

Acknowledgements

This research was financially sponsored by the School of Mechanical and Aerospace Engineering, Nanyang Technological University. The authors would like to sincerely express their gratitude to the laboratory technicians at the Energy Systems, Computer-Aided Engineering and the Manufacturing laboratories of Nanyang Technological University for their technical assistance. The authors are grateful to Dr Goh Aik Ling for providing feedback on the initial research direction of this project.

References

1. Agostini, B., et al., *State of the Art of High Heat Flux Cooling Technologies.* Heat Transfer Engineering, 2007. **28**(4): p. 258-281.
2. Khan, M.G. and A. Fartaj, *A review on microchannel heat exchangers and potential applications.* International Journal of Energy Research, 2011. **35**(7): p. 553-582.
3. Ghaedamini, H., P.S. Lee, and C.J. Teo, *Developing forced convection in converging–diverging microchannels.* International Journal of Heat and Mass Transfer, 2013. **65**: p. 491-499.
4. Karayiannis, T.G. and M.M. Mahmoud, *Flow boiling in microchannels: Fundamentals and applications.* Applied Thermal Engineering, 2017. **115**: p. 1372-1397.

5. Kandlikar, S.G., et al., *Heat transfer in microchannels—2012 status and research needs.* Journal of Heat Transfer, 2013. **135**(9): p. 091001.
6. Goodling, J.S. *Microchannel heat exchangers: a review.* in *SPIE's 1993 International Symposium on Optics, Imaging, and Instrumentation*. 1993. SPIE.
7. Palm, B., *Heat transfer in microchannels.* Microscale Thermophysical Engineering, 2001. **5**(3): p. 155-175.
8. Sui, Y., et al., *Fluid flow and heat transfer in wavy microchannels.* International Journal of Heat and Mass Transfer, 2010. **53**(13): p. 2760-2772.
9. Mohammed, H.A., P. Gunnasegaran, and N.H. Shuaib, *Numerical simulation of heat transfer enhancement in wavy microchannel heat sink.* International Communications in Heat and Mass Transfer, 2011. **38**(1): p. 63-68.
10. Gong, L., et al., *Parametric Numerical Study of Flow and Heat Transfer in Microchannels With Wavy Walls.* Journal of Heat Transfer, 2011. **133**(5): p. 051702-051702-10.
11. Xie, G., et al., *Constructal Theory Based Geometric Optimization of Wavy Channels in the Low Reynolds Number Regime.* Journal of Electronic Packaging, 2014. **136**(3): p. 031013-031013-8.
12. Rostami, J., A. Abbassi, and M. Saffar-Avval, *Optimization of conjugate heat transfer in wavy walls microchannels.* Applied Thermal Engineering, 2015. **82**: p. 318-328.
13. Hung, T.-C. and W.-M. Yan, *Effects of tapered-channel design on thermal performance of microchannel heat sink.* International Communications in Heat and Mass Transfer, 2012. **39**(9): p. 1342-1347.
14. Ho, C.J., et al., *Thermal and hydrodynamic characteristics of divergent rectangular minichannel heat sinks.* International Journal of Heat and Mass Transfer, 2018. **122**: p. 264-274.
15. Sakanova, A., C.C. Keian, and J. Zhao, *Performance improvements of microchannel heat sink using wavy channel and nanofluids.* International Journal of Heat and Mass Transfer, 2015. **89**: p. 59-74.
16. Leng, C., et al., *Multi-parameter optimization of flow and heat transfer for a novel double-layered microchannel heat sink.* International Journal of Heat and Mass Transfer, 2015. **84**: p. 359-369.
17. Harikrishnan, S. and S. Tiwari, *Effect of skewness on flow and heat transfer characteristics of a wavy channel.* International Journal of Heat and Mass Transfer, 2018. **120**: p. 956-969.
18. Abdul Hasis, F.B., et al., *Thermo hydraulic performance analysis of twisted sinusoidal wavy microchannels.* International Journal of Thermal Sciences, 2018. **128**: p. 124-136.
19. Lin, L., et al., *Heat transfer enhancement in microchannel heat sink by wavy channel with changing wavelength/amplitude.* International Journal of Thermal Sciences, 2017. **118**: p. 423-434.
20. Dominic, A., et al., *An experimental study of heat transfer and pressure drop characteristics of divergent wavy minichannels using nanofluids.* Heat and Mass Transfer, 2017. **53**(3): p. 959-971.
21. Khoshvaght-Aliabadi, M. and M. Sahamiyan, *Performance of nanofluid flow in corrugated minichannels heat sink (CMCHS).* Energy Conversion and Management, 2016. **108**: p. 297-308.
22. Ho, C.J., et al., *A combined numerical and experimental study on the forced convection of Al2O3-water nanofluid in a circular tube.* International Journal of Heat and Mass Transfer, 2018. **120**: p. 66-75.

23. Bouremel, Y., et al., *Characterization of counter-rotating streamwise vortices in flat rectangular channel with one-sided wavy wall.* Experimental Thermal and Fluid Science, 2017. **82**: p. 75-82.
24. Cheng, K.X., Y.S. Chong, and K.T. Ooi, *Thermal-hydraulic performance of a tapered microchannel.* International Communications in Heat and Mass Transfer, 2018. **94**: p. 53-60.
25. Goh, A.L. and K.T. Ooi, *Nature-inspired Inverted Fish Scale microscale passages for enhanced heat transfer.* International Journal of Thermal Sciences, 2016. **106**: p. 18-31.
26. Goh, A.L. and K.T. Ooi, *Scale-inspired enhanced microscale heat transfer in macro geometry.* International Journal of Heat and Mass Transfer, 2017. **113**: p. 141-152.
27. Foo, Z.H., et al., *Single-phase convective heat transfer performance of wavy microchannels in macro geometry.* Applied Thermal Engineering, 2018. **141**: p. 675-687.
28. Cheng, K.X. and K.T. Ooi, *Investigation of effect of protrusion height on microscale heat transfer and fluid flow in macro geometries.* Applied Thermal Engineering, 2017. **118**: p. 244-255.
29. Kong, K.S. and K.T. Ooi, *A numerical and experimental investigation on microscale heat transfer effect in the combined entry region in macro geometries.* International Journal of Thermal Sciences, 2013. **68**: p. 8-19.
30. Ebrahimian, M. and G.R. Ansarifar, *Investigation of the nano fluid effects on heat transfer characteristics in nuclear reactors with dual cooled annular fuel using CFD (Computational Fluid Dynamics) modeling.* Energy, 2016. **98**: p. 1-14.
31. Porto, M.P., et al., *Boiling heat transfer on a simulated nuclear fuel rod with annular fins.* International Journal of Heat and Mass Transfer, 2014. **68**: p. 29-34.
32. Guo, Z.Y., D.Y. Li, and B.X. Wang, *A novel concept for convective heat transfer enhancement.* International Journal of Heat and Mass Transfer, 1998. **41**(14): p. 2221-2225.
33. Churchill, S.W., *A comprehensive correlating equation for laminar, assisting, forced and free convection.* AIChE Journal, 1977. **23**(1): p. 10-16.
34. Lemmon, E.W., *NIST reference fluid thermodynamic and transport properties—REFPROP*. 2002.
35. Wagner, W. and A. Pruß, *The IAPWS formulation 1995 for the thermodynamic properties of ordinary water substance for general and scientific use.* Journal of physical and chemical reference data, 2002. **31**(2): p. 387-535.
36. ANSYS, *CFX Solver Theory Guide*. . Inc., Canonsburg, PA, 2011.
37. Rogers, S., et al. *A comparison of turbulence models in computing multi-element airfoil flows*. in *32nd Aerospace Sciences Meeting and Exhibit*. 1994.
38. Shah, R.K. and A.L. London, *Chapter VI - Parallel Plates*, in *Laminar Flow Forced Convection in Ducts*. 1978, Academic Press. p. 153-195.
39. Muzychka, Y.S., *Analytical and experimental study of fluid friction and heat transfer in low Reynolds number flow heat exchangers*. 1999: University of Waterloo.
40. Tao, W.-Q., Z.-Y. Guo, and B.-X. Wang, *Field synergy principle for enhancing convective heat transfer—its extension and numerical verifications.* International Journal of Heat and Mass Transfer, 2002. **45**(18): p. 3849-3856.